Polarization Dependence of Plasmonic Nanotoroid Dimer Antenna

Magda O. El-Shenawee, *Senior Member, IEEE*

***Abstract*—The surface Plasmon resonance of nanotoroid dimer antenna immersed in air is investigated. The method-of-moments surface integral equation is employed to compute the resonance wavelength and the enhanced electric field of the nanoantenna. The results show that the size of the gap causes redshift to the resonance wavelength of the dominant mode only when the incident polarization is parallel to the axis of the dimer. The dominant mode is a symmetric mode, and the higher order mode is a combination of symmetric and antisymmetric modes.**

***Index Terms*—Gold optical properties, nanotoroid dimer antenna, optical antennas, plasmonic antennas, polarization.**

I. Introduction

NANOANTENNAS, also known as *optical antennas*, have recently attracted the interest of the engineering community for their potential applications in solar collectors, IR and DNA detectors, biosensors, and terahertz imaging sensors. Nanostructures with sizes ranging from 30 to 100 nm and in a variety of shapes were studied [1]–[8]. These nanoantennas resonate at few hundreds of nanometers depending on their material and dimensions.

Several important aspects of nanoantennas were investigated in the literature. Romero *et al.* discussed the physical and unphysical modes of the nanoparticle dimer [1]. Rechberger *et al.* investigated the electromagnetic interactions between closely spaced nanoparticles [2]. The input impedance, radiation resistance, and impedance matching of plasmonic optical dimer were presented by Alù *et al.* [3]. Lassiter *et al.* investigated the polarization dependence of nonsymmetric nanoshells [4].

The single nanoring was studied in several works [5]–[8]. The *symmetric* mode solution was obtained using the boundary element method, slab-like model, and experimental data [5]. In this mode, the pattern of oscillations is associated with a charge distribution of the same sign at the inner and outer surfaces of the ring wall. In [6], Mary *et al.* presented a quasi-static expression supported with experimental results for a single nanotorus on a substrate for the planar and normal polarizations.

Dutta *et al.* presented the plasmon hybridization method to investigate the properties of toroids of different shapes and polarizations [7] where the plasmons of higher order modes were studied. Hao *et al.* presented an experimental and theoretical analysis of gold nanorings showing that the dark modes at normal incidence were observed at oblique incidence [8]. As reported in [5]–[8], when changing the inner to the outer radii ratio, the nanoring can exhibit tunable resonances that are not the case for solid nanoparticles.

The current work investigates the surface Plasmon resonance and the enhanced fields of the dominant and the higher order modes of a nanotoroid dimer antenna immersed in air (see Fig. 1).

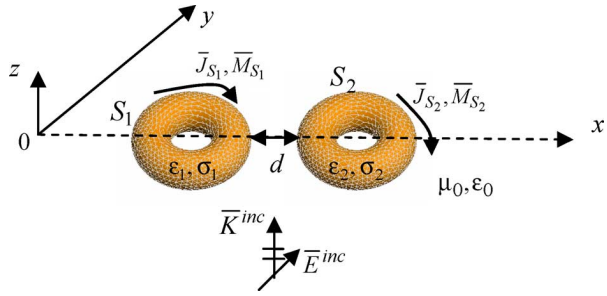

Fig. 1. Nanotoroid dimer antenna with the incident plane waves $\overline{K}^{\text{inc}}$ in the z-direction. The figure shows the perpendicular polarization case.

II. Methodology

At optical frequencies, gold demonstrates negative real part of permittivity with debatable values among published data [9]–[11]. This controversy in the optical properties of gold has influenced the modeled resonance behavior of gold nanoantennas. Interpolated data based on Johnson *et al.* experimental optical properties of gold are adopted in this work [9].

The method-of-moments surface integral equation (MoM/SI) is employed to calculate the electric $(\overline{J}_{S_k})$ and the magnetic $(\overline{M}_{S_k})$ surface current densities on the surface of the nanotoroid dimer antenna, $k = 1, 2$, shown in Fig. 1. The near and far electric and magnetic fields, $\overline{E}$ and $\overline{H}$, can be easily obtained once the current densities are calculated [12].

III. Numerical Results

In this section, the surrounding medium is assumed to be air. Each toroid is made of gold with outer and inner radii of 42 and 21 nm, respectively. The antenna gap is of size d that ranges from 0 to 366 nm. Plane waves of amplitude 1 V/m and wavelength ranges from 200 to 800 nm are employed to excite the nanoantenna. The incident electric field is polarized in the y-direction in all cases presented here. When the antenna's axis is aligned in the x-direction as shown in Fig. 1, the case is defined as perpendicular polarization where the incident electric field is perpendicular to the x-axis. When the antenna's axis is aligned in the y-direction (upon rotating Fig. 1 by 90°), the case is defined as parallel polarization, in which the electric field is parallel to the axis of the antenna.

Manuscript received March 26, 2010; revised May 05, 2010; accepted May 14, 2010. Date of publication May 20, 2010; date of current version June 03, 2010. This work was supported in part by National Science Foundation (NSF) Grant ECS-0524042.

The author is with the Electrical Engineering Department, University of Arkansas, Fayetteville, AR 72701 USA (e-mail: magda@uark.edu).

Color versions of one or more of the figures in this letter are available online at http://ieeexplore.ieee.org.

Digital Object Identifier 10.1109/LAWP.2010.2050853

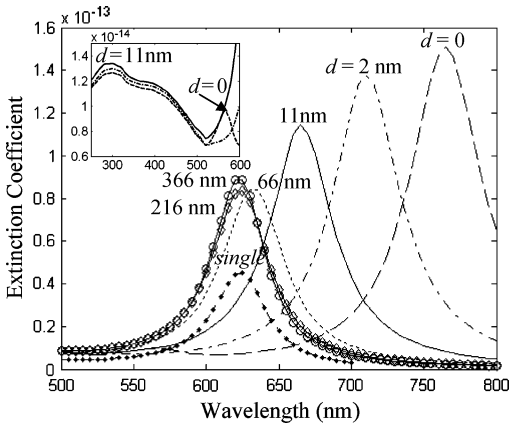

Fig. 2. Extinction coefficient versus wavelength for parallel polarization for different gap sizes d. The inset shows the higher order modes for $d = 0$, 2, 11 nm.

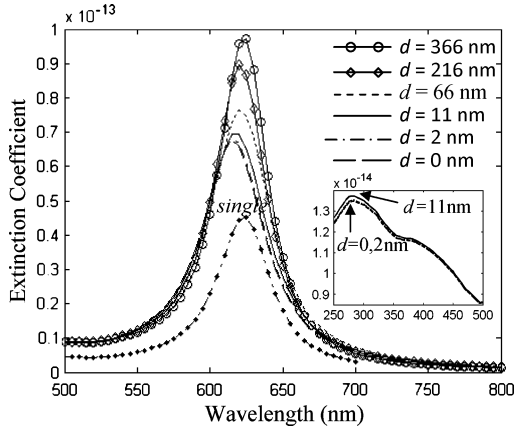

Fig. 3. Extinction coefficient versus wavelength for perpendicular polarization for different gap sizes d. The inset shows the higher order modes for $d = 0$, 2, 11 nm.

Each toroid is discretized into 800 nodes and 1600 triangular patches to produce 2400 edges. This implies that each toroid represents 2400 unknown electric current coefficients and 2400 unknown magnetic current coefficients. The total number of unknowns becomes 9600 in this case. All computations were conducted on HP server using a single processor of 1 GHz clock and 4 GB RAM. The average CPU time required per frequency ranges from 30 min to 1 h. The wavelength is sampled at 5 nm to capture the resonance wavelengths.

Fig. 2 shows the extinction coefficient versus the wavelength for the parallel polarization with the nanoantenna's axis in Fig. 1 rotated 90° to be in the y-direction. The extinction coefficient's asymptotic expression is given by [13]

$$C_{\text{ext}} = 2\lambda_0 \text{Img.} \left(\overline{\overline{E}}^{\text{inc}} \cdot \overline{\overline{E}}^{\text{sca}} \Big|_{\hat{n}^{\text{sca}} = \hat{n}^{\text{inc}}} \right) \tag{1}$$

where $\overline{E}^{\text{inc}} = \overline{\overline{E}}^{\text{inc}}(e^{jk_0 r}/r)$ and $\overline{E}^{\text{sca}} = \overline{\overline{E}}^{\text{sca}}(e^{jk_0 r}/r)$ are the incident and scattered electric fields, respectively, $\hat{n}^{\text{inc}}$ and $\hat{n}^{\text{sca}}$ are the unit vectors in the incident and scatter directions, respectively, and λ_0 is the wavelength in air. The extinction coefficient of a single toroid of the same dimensions is plotted in Fig. 2 for comparison.

The results of Fig. 2 demonstrate a significant effect of the gap size d on the surface Plasmon resonances of the nanoantenna. The resonance of the dominant mode is redshifted as the gap size increases. In addition, the amplitude of the extinction coefficient decreases with the increase of the gap size d from 0 to 66 nm. However, as d increases from 66 to 366 nm, the resonance appears to occur almost at the same wavelength ~617 nm of a single toroid [6]. As d increases, e.g. 366 nm, the dimer resonates at the same frequency of a single toroid. The amplitude of the extinction coefficient, however, becomes almost double that of a single toroid as shown in Fig. 2. Clearly, the multiple interactions between the two toroids decrease with the increase of the gap size.

The MoM/SI computer code is in very good agreement with the Mie solution of a 60-nm radius gold nanoparticle [14]. The algorithm was also validated with the commercial package FEKO and with other MoM/SI computer codes. For a single nanotoroid, the resonance wavelength results reasonably agreed with [6], while the amplitude of the extinction coefficient was smaller. This discrepancy could be due to the difference in the optical properties of gold. The current work used interpolated data based on Johnson *et al.* [9], while the work in [6] used data from Palik [10]. A comparison of the extinction coefficients of single toroid using the gold properties of [9]–[11] revealed differences in both the amplitude and the resonance wavelength.

The results of Fig. 3 show the extinction coefficient versus the wavelength for the perpendicular polarization (see Fig. 1). Interestingly, insignificant shift is observed in the resonance wavelength when the gap size increases (i.e., only few nanometers that could be due to *numerical* accuracy). In addition, the amplitude of the extinction efficient increases with the increase of the gap size d. At $d = 366$ nm, the amplitude of the extinction coefficient becomes almost double that of a single toroid, similar to the parallel polarization in Fig. 2.

The results of Figs. 2 and 3 show the resonance wavelength of the *dominant* modes, while the insets in both figures show the resonance wavelengths of *higher order* modes. For example, in the parallel polarization when $d = 0$, a higher order mode is observed at ~565 nm, and when $d = 11$ nm, a higher order mode is observed at ~300 nm (see Fig. 2). For the perpendicular mode, a higher order mode at ~280 nm is observed when $d = 11$ nm (see Fig. 3), etc. Due to the large imaginary part of the gold dielectric constant at these frequencies, the extinction coefficients of the higher order modes exhibit much smaller amplitudes compared to those of the dominant modes.

Fig. 4 shows the amplitude of the enhanced scattered electric field in the xy plane at $z = 30$ nm above the dimer for the parallel polarization case. Three values of the gap size are shown as $d = 0$, 2 , and 11 nm. All results in Fig. 4 considered the dominant modes. The results in Fig. 4(b)–(d) show that the fields are enhanced at two spots (dark gray) above the toroids where the field intensity is ~7.5 V/m when $d = 0$, 7 V/m when $d = 2$ nm, and 6 V/m when $d = 11$ nm. It will be shown later in this section that these two maximum field intensity spots correspond to the location where the same sign surface charges exist on the inner and outer walls of each toroid of the dimer.

Fig. 4(b)–(d) show that the field intensity in the antenna gap depends on the gap size. In Fig. 4(c), a field intensity of ~3.5 V/m is observed when gap size is 2 nm, and in Fig. 4(d), an intensity of ~4.5 V/m is observed in the gap when the gap size is 11 nm. When the two toroids touch each other in

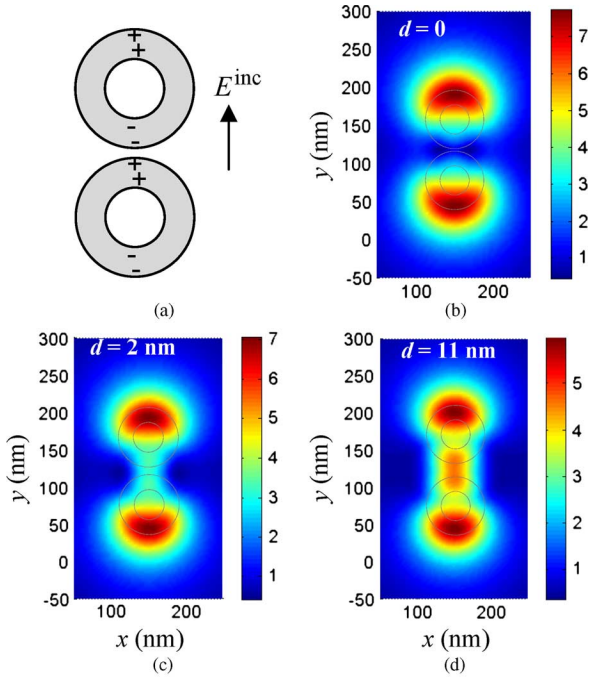

Fig. 4. (a) Sketch of the *symmetric* mode. For the dominant mode, the near scattered electric fields (V/m) in the xy plane at 30 nm above the nanotoroid dimer antenna for (b) $\lambda_0 = 764$ nm ($d = 0$), (c) $\lambda_0 = 710$ nm ($d = 2$ nm), and (d) $\lambda_0 = 664$ nm ($d = 11$ nm). Parallel polarization.

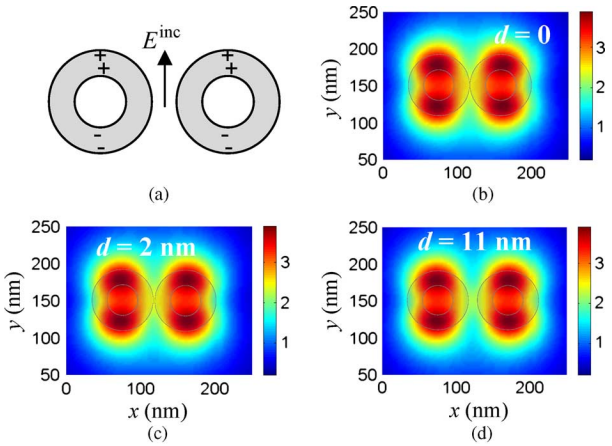

Fig. 5. (a) Sketch of *symmetric* mode. For the dominant mode, the near scattered electric fields (V/m) in the xy plane at 30 nm above the nanotoroid dimer antenna at $\lambda_0 \sim 617$ nm for (b) $d = 0$, (c) $d = 2$ nm, and (d) $d = 11$ nm. Perpendicular polarization.

Fig. 4(b), minimum field is observed in the gap due to the possible cancellation of surface charges on the touching toroids' wall surfaces.

For the parallel polarization, the incident electric field in the gap is normal to the toroids' wall surfaces consistent with the charge signs in Fig. 4(a). As the gap size increases, the equivalent capacitance value decreases. As a result, the resonance wavelength of a simple equivalent LC circuit decreases. This concept is consistent with the results observed in Fig. 2.

For the perpendicular polarization case, Fig. 5 shows the amplitude of the scattered near electric fields in the xy plane at $z = 30$ nm for the same gap sizes of Fig. 4. Fig. 5(a) shows the sketch of the *symmetric* mode. Fig. 5(b)–(d) show two spots of maximum field intensities above each toroid at the locations of same sign surface charges on the inner and outer walls. The

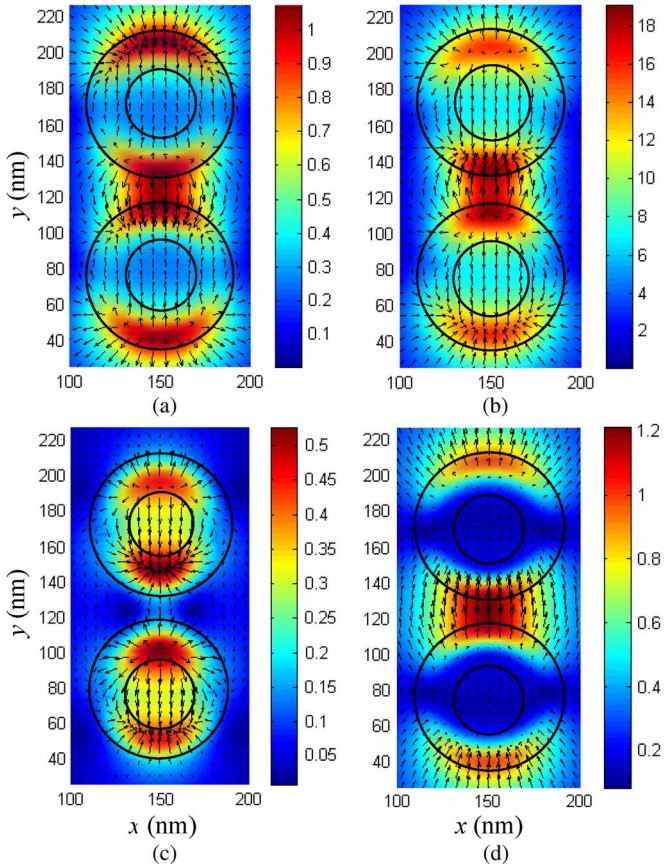

Fig. 6. (a) Real part and (b) imaginary part of *dominant* mode with resonance wavelength 664 nm. (c) Real part and (d) imaginary part of *higher order* mode with wavelength 300 nm (inset of Fig. 2). Parallel polarization $d = 11$ nm.

maximum amplitude is ~4 V/m regardless of the gap size in Fig. 5(b)–(d). Also, in all these figures, the field intensity at the center of each toroid is ~3 V/m. It is interesting to observe that for the perpendicular polarization both the surface Plasmon resonance and the maximum field intensities are insensitive to the gap size, which was not the case for the parallel polarization in Fig. 4.

For the perpendicular polarization, the incident electric field in the gap is parallel to the toroids' wall surfaces. Accordingly, there is no effective capacitance caused by the gap. This scenario could explain the insignificant effect of the gap size on the resonant wavelength observed in Fig. 3.

As discussed in [5] and [7], the *symmetric* mode exhibits a charge distribution of the same sign at the inner and outer surfaces of the single toroid walls as shown in Figs. 4(a) and 5(a) for the dimer case. The work of [7] studied the possible charge distributions of higher order modes including the *antisymmetric* mode where the inner and outer walls exhibit opposite sign charges.

In order to investigate the charge distribution of the modes, the flux lines are plotted for the real and imaginary parts of the scattered electric fields. The fields are plotted in the xy plane at $z = 15$ nm (i.e., 3 nm above the dimer) for $d = 11$ nm. Fig. 6(a) and (b) show the real and imaginary parts of the electric fields for the *dominant* mode at wavelength 664 nm, while Fig. 6(c) and (d) show the real and imaginary parts at wavelength 300 nm, which is the resonance of the *higher order* mode when $d = 11$ nm as shown in Fig. 2.

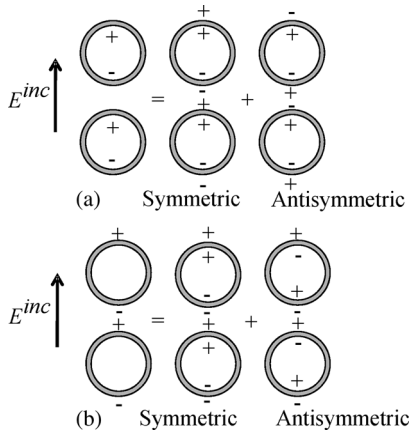

Fig. 7. Illustrative sketch of surface charges for higher order mode observed in (a) the inner surface wall of Fig. 6(c) and (b) the outer surface wall of Fig. 6(d). Parallel polarization.

The direction of the flux lines indicates to the positive or negative charge distribution. Fig. 6(a) shows that for the *dominant* mode, the real part of the field is much smaller than that of the imaginary part ($\sim$1.2 V/m versus 19 V/m). Both the real and imaginary parts exhibit maximum field intensities in the gap, but of different values. The flux lines of the real part in Fig. 6(a) seem to exhibit same charge signs at the inner and outer surface walls of the dimer as negatives at the upper part, positives right above the gap, negatives right below the gap, and positive charges at the lower part of the dimer.

The flux lines of the imaginary part in Fig. 6(b) seem also to exhibit the same sign charges as positives at the upper part of the dimer, negatives right above the gap, positives right below the gap, and negatives at the lower part of the dimer. The results of Fig. 6(a) and (b) indicate that the *dominant* mode of the dimer is indeed a *symmetric* type mode.

The results of Fig. 6(c) and (d) show the flux lines of the real and imaginary parts, respectively, of the higher order mode at the resonance wavelength of 300 nm shown in Fig. 2. Fig. 6(c) seems to indicate that mainly the inner walls of each toroid exhibit charge distribution as positive at the first toroid upper inner wall ($\sim y = 190$ nm), negative at the first toroid lower inner wall ($\sim y = 150$ nm), positive at the second toroid upper inner wall $\sim y = 95$ nm, and negative at the second toroid lower inner wall $\sim$ y $=$ 60 nm.

On the other hand, the flux lines in Fig. 6(d) seem to indicate that mainly the outer walls of each toroid exhibit charge distribution as positive at the first toroid upper outer wall ($\sim y = 210$ nm), negative at the outer wall right above the gap ($\sim y = 130$ nm), positive at the outer wall below the gap ($\sim y = 115$ nm), and negative at the lower outer wall of the dimer ($\sim y = 35$ nm).

Notice the lack of flux lines around the dimer in Fig. 6(c), even in the gap, and inside the centers of both toroids in Fig. 6(d). To explain this observation, an illustrative sketch of surface charges on the walls is given in Fig. 7(a) for the real part of the field of Fig. 6(c) and in Fig. 7(b) for the imaginary part of the field of Fig. 6(d).

The illustrative sketch in Fig. 7(a) and (b) indicate that the *higher order* mode at resonance wavelength 300 nm is composed of a *symmetric* type and a *antisymmetric* type mode, based on their charge distributions. This sketch could be used to explain the reason the *antisymmteric* mode could not individually observed. This concept is similar to what Hao *et al.* used to explain the *dark modes* in [8]. Similar observation for the perpendicular polarization was noticed when $d = 11$ nm at the resonance wavelength of 280 nm shown in the inset of Fig. 3.

The radiation pattern of the nanoantenna was consistent with the well-known radiation pattern of a dipole antenna "donut shape" (not shown).

IV. Conclusion

The current work investigated the surface plasmon resonance and the enhanced fields of the dominant and the higher order modes of a nanotoroid dimer antenna immersed in air. The results showed a redshift in the resonance wavelength of the dominant modes only when the incident polarization was parallel to the dimer's axis. The results demonstrated that the dominant mode is indeed a *symmetric*-type mode and the higher order mode is a combination of *symmetric*- and *antisymmetric*-type modes.

For the normal polarization (i.e., the electric field is normal to the plane of the dimer), the extinction coefficients exhibited much smaller amplitudes when compared to those of the planar polarizations considered in this work as reported in [6], [7], and [14]. Also, increasing the refractive index of the surrounding medium could influence the resonance wavelength as reported in [6].

References

[1] I. Romero, J. Aizpurua, G. W. Bryant, and F. J. Garcia de Abajo, "Plasmon in nearly touching metallic nanoparticles: Singular response in the limit of touching dimmers," *Opt. Express*, vol. 14, no. 21, pp. 9988–9999, 2006.

[2] W. Rechberger, A. Hohenau, A. Leitner, J. R. Krenn, B. Lamprecht, and F. R. Aussenegg, "Optical properties of two interacting gold nanoparticles," *Opt. Commun.*, vol. 220, pp. 137–141, 2003.

[3] A. Alù and N. Engheta, "Hertzian plasmonic nanodimer as an efficient optical nanoantenna," *Phys. Rev. B*, vol. 78, pp. 195111–195116, 2008.

[4] J. B. Lassiter, M. W. Knight, N. A. Mirin, and N. J. Halas, "Reshaping the plasmonic properties of an individual nanoparticle," *Nano Lett.*, vol. 9, no. 12, pp. 4326–4332, 2009.

[5] J. Aizpurua, P. Hanarp, D. Sutherland, M. Kall, G. Bryant, and F. Abajo, "Optical properties of gold nanorings," *Phys. Rev. Lett.*, vol. 90, no. 5, pp. 057401-1–057401-4, February 7, 2003.

[6] A. Mary, D. M. Koller, A. Hohenau, J. R. Krenn, A. Bouhelier, and A. Dereux, "Optical absorption of torus-shaped metal nanoparticles in the visible range," *Phys. Rev. B*, vol. 76, pp. 245422-(1)–245422-(5), 2007.

[7] C. M. Dutta, T. A. Ali, D. W. Brandl, T. H. Park, and P. Nordlander, "Plasmonic properties of a metallic torus," *J. Chem. Phys.*, vol. 129, pp. 084706-1–084706-9, 2008.

[8] F. Hao, E. M. Larsson, T. A. Ali, D. S. Sutherland, and P. Nordlander, "Shedding light on dark plasmons in gold nanorings," *Chem. Phys. Lett.*, vol. 458, pp. 262–266, 2008.

[9] P. B. Johnson and R. W. Christy, "Optical constants of the noble metals," *Phys. Rev. B*, vol. 6, no. 12, pp. 4370–4379, 1972.

[10] E. D. Palik, *Handbook of Optical Constants of Solids*. New York: Academic, 1985.

[11] H.-J. Hagemann, W. Gudat, and C. Kunz, "Optical constants from the far infrared to the X-ray region: Mg, Al, Cu, Ag, Au, Bi, C, and A1203," *J. Opt. Soc. Amer.*, vol. 65, no. 6, pp. 742–744, Jun. 1975.

[12] M. El-Shenawee, "Scattering from multiple objects buried under two-dimensional randomly rough surface using the steepest descent fast multipole method," *IEEE Trans. Antennas Propag.*, vol. 51, no. 4, pp. 802–809, Apr. 2003.

[13] M. Born and E. Wolf, *Principles of Optics*, 4th ed. New York: Pergamon, 1970, ch. 13, p. 658.

[14] M. El-Shenawee, D. Macias, A. Baudrion, and R. Bachelot, "Torus nano-antenna: Enhanced field and radiation pattern," in *Proc. IEEE Antenn. Propag. USNC/URSI*, Charleston, SC, Jun. 1–5, 2009, pp. 1–4.